Robust A_1 superconductivity in the kagome lattice

Yi Gao

Center for Quantum Transport and Thermal Energy Science, Jiangsu Key Lab on Opto-Electronic Technology, School of Physics and Technology, Nanjing Normal University, Nanjing 210023, China

(Received 16 January 2024; revised 21 April 2024; accepted 20 May 2024; published 3 June 2024)

We theoretically studied the superconducting pairing in a single-orbital kagome lattice. By taking the electron-electron correlation as the pairing mechanism, we obtained the spin and charge fluctuations based on the random-phase approximation and calculated the preferred pairing function based on the linearized Eliashberg equation. It turns out that the frequency dependence of the Eliashberg equation is of great importance in this model, and may lead to spin-triplet and odd-frequency pairing state. We further found a robust A_1 pairing symmetry, with respect to the correlation strength and Fermi surface variation. This pairing state does not break the time-reversal symmetry and can be nodal or nodeless. We concluded that, in the recently discovered kagome superconductors, the preferred pairing symmetry is A_1, even if the pairing originates from the electron-electron interaction.

DOI: 10.1103/PhysRevB.109.214501

I. INTRODUCTION

Recently, superconductivity has been found in a series of materials AV_3Sb_5 ($A = \mathrm{K}, \mathrm{Rb}, \mathrm{Cs}$) featuring the kagome lattice structure [1–7]. These discoveries soon attracted much attention among physics communities, because the kagome band structures are very special. They host flat bands, Dirac cones, and van Hove singularities at various electron fillings, making them particularly suitable for studying the nontrivial band topology, exotic Fermi surface instabilities, and superconductivity, as well as their interplay. Indeed, the normal state band structures of the above kagome superconductors are argued to feature a $\mathbb{Z}_2$ topological invariant [1,3], and a charge density wave (CDW) has also been observed [8–13].

Regarding the superconductivity, it has been widely observed that superconductivity gets enhanced once CDW is suppressed by either doping [14–20] or pressure [5,6,21], suggesting a competition between these two orders. However currently there is no consensus about the superconducting pairing symmetry. Some experiments suggest that the pairing is nodal [22,23], while others indicate a nodeless pairing [24–29], or even a nodal to nodeless transition [30]. In addition, whether the superconducting state itself breaks the time-reversal symmetry is also controversial [30,31].

On the theoretical side, various superconducting pairing mechanisms and symmetries have been proposed. The pairing mechanisms are argued to be electron-phonon interaction [32–34] or electron-electron correlation [35–41]. While the former usually leads to conventional s-wave pairing symmetry with a full gap structure [32,33], the latter, on the other hand, predicts a variety of pairing symmetries, including s wave, p wave, f wave, and even $d_{x^2-y^2} + id_{xy}$ wave that breaks the time-reversal symmetry [35–41]. In addition, these pairing symmetries and the gap nodes are very sensitive to the strength of the electron correlation, as well as to a slight change of the Fermi surface. Therefore, a comparison between the theoretical and experimental pairing symmetries is difficult.

In this work, we also study the pairing symmetries in the kagome lattice, when the Fermi level is slightly away from the upper van Hove singularity, as in the above mentioned kagome superconductors. We consider the electron-electron correlation as the pairing mechanism, and solve the linearized Eliashberg equation to obtain a sublattice-, momentum- and frequency-dependent pairing function. We found a robust A_1 pairing symmetry that is not sensitive to the correlation strength and Fermi surface shape, together with a possible A_1 odd-frequency triplet pairing in the phase space. In all we obtained pairing functions that are real and do not break the time-reversal symmetry. Complex pairing functions that do break the time-reversal symmetry remain subleading and are not the leading pairing function.

II. METHOD

We adopt a single-orbital tight-binding model of the kagome lattice [36–40]. The noninteracting part of the Hamiltonian can be written as $H_0 = \sum_{\mathbf{k}\sigma} \psi^\dagger_{\mathbf{k}\sigma} M_{\mathbf{k}} \psi_{\mathbf{k}\sigma}$, where $\psi^\dagger_{\mathbf{k}\sigma} = (c^\dagger_{\mathbf{k}A\sigma}, c^\dagger_{\mathbf{k}B\sigma}, c^\dagger_{\mathbf{k}C\sigma})$ and

$$M_{\mathbf{k}} = \begin{pmatrix} -\mu & \epsilon_{AB,\mathbf{k}} & \epsilon_{AC,\mathbf{k}} \\ \epsilon^*_{AB,\mathbf{k}} & -\mu & \epsilon_{BC,\mathbf{k}} \\ \epsilon^*_{AC,\mathbf{k}} & \epsilon^*_{BC,\mathbf{k}} & -\mu \end{pmatrix}. \tag{1}$$

Here $c^\dagger_{\mathbf{k}s\sigma}$ creates a spin σ ($\sigma = \uparrow, \downarrow$) electron with momentum $\mathbf{k}$ on the sublattice s ($s = A, B, C$). In addition,

$$\begin{aligned} \epsilon_{AB,\mathbf{k}} &= -[1 + e^{-i(k_1 - k_2)}], \\ \epsilon_{AC,\mathbf{k}} &= -(1 + e^{-ik_1}), \\ \epsilon_{BC,\mathbf{k}} &= -(1 + e^{-ik_2}), \end{aligned} \tag{2}$$

where $k_1 = \mathbf{k} \cdot \mathbf{a}_1$ and $k_2 = \mathbf{k} \cdot \mathbf{a}_2$, with $\mathbf{a}_1$ and $\mathbf{a}_2$ being the primitive

vectors of the kagome lattice, which are

$$\mathbf{a}_1 = (1, 0),$$
$$\mathbf{a}_2 = \left(\frac{1}{2}, \frac{\sqrt{3}}{2}\right). \tag{3}$$

Throughout this work, we take the nearest-neighbor hopping integral as the energy unit and the lattice constant of the unit cell as the length unit.

The interaction Hamiltonian can be written as $H_{\text{int}} = H_{\text{onsite}} + H_{NN}$ [35–38,40], where

$$H_{\text{onsite}} = U \sum_{i,s} n_{is\uparrow} n_{is\downarrow}, \tag{4}$$

and

$$H_{NN} = \frac{V}{2} \sum_{i,s,i',s',\sigma,\sigma'} n_{is\sigma} n_{i's'\sigma'}. \tag{5}$$

In Eqs. (4) and (5), $n_{is\sigma} = c^{\dagger}_{is\sigma} c_{is\sigma}$ is the electron number operator with spin σ at the sublattice s of the unit cell i and (i', s') represents a lattice site which is a nearest-neighbor of the lattice site (i, s).

The irreducible susceptibility is defined as Eq. (A1) and can be expressed as [35]

$$\chi_0^{\alpha\beta,\gamma\delta}(q) = -\frac{T}{N} \sum_k G^{\gamma\beta}(k+q) G^{\alpha\delta}(k), \tag{6}$$

where $G(k) = (ip_n I - M_{\mathbf{k}})^{-1}$ is the normal Green's function matrix, I is the unit matrix, T is the temperature and N is the number of unit cells. Here $q = (\mathbf{q}, i\omega_n)$ and $k = (\mathbf{k}, ip_n)$, with $\omega_n = 2n\pi T$ and $p_n = (2n-1)\pi T$.

If an infinite number of p_n are considered in the summation of Eq. (6), then the frequency summation can be done analytically, which gives [35]

$$\chi_0^{\alpha\beta,\gamma\delta}(q) = -\frac{1}{N} \sum_{\mathbf{k},\eta,\nu} Q^{\gamma\eta}_{\mathbf{k}+\mathbf{q}} Q^{*\beta\eta}_{\mathbf{k}+\mathbf{q}} Q^{\alpha\nu}_{\mathbf{k}} Q^{*\delta\nu}_{\mathbf{k}} \times \frac{f\left(E^{\nu}_{\mathbf{k}}\right) - f\left(E^{\eta}_{\mathbf{k}+\mathbf{q}}\right)}{i\omega_n + E^{\nu}_{\mathbf{k}} - E^{\eta}_{\mathbf{k}+\mathbf{q}}}. \tag{7}$$

Here $E^{\nu}_{\mathbf{k}}$ is the νth eigenvalue of $M_{\mathbf{k}}$ in Eq. (1) and $Q_{\mathbf{k}}$ is a unitary matrix that diagonalizes $M_{\mathbf{k}}$. Finally, $f(x) = 1/(e^{x/T} + 1)$ is the Fermi distribution function.

Within the random-phase approximation (RPA), the spin and charge susceptibilities $\chi_s(q)$ and $\chi_c(q)$ can be calculated by Eq. (A2) [35].

Close to T_c, the linearized Eliashberg equation can be expressed as [42]

$$\lambda \phi^{\delta\beta}(k) = -\frac{T}{N} \sum_q \sum_{\alpha,\gamma,\eta,\nu} G^{\alpha\gamma}(k-q) G^{\nu\eta}(q-k) \times V^{\nu\beta,\alpha\delta}(q) \phi^{\gamma\eta}(k-q), \tag{8}$$

where $\phi(k)$ is the anomalous self-energy, and the pairing interaction $V(q)$ is

$$\tfrac{1}{2}[3U_s \chi_s(q) U_s - C(\mathbf{q}) \chi_c(q) C(\mathbf{q}) + U_s + C(\mathbf{q})] \tag{9}$$

for spin singlet pairing and

$$-\tfrac{1}{2}[U_s \chi_s(q) U_s + C(\mathbf{q}) \chi_c(q) C(\mathbf{q}) - U_s - C(\mathbf{q})] \tag{10}$$

for spin triplet pairing. At this stage, the derivation is standard without qualitative difference with respect to previous studies [35,36,41]. However, instead of neglecting the frequency dependence of $\phi(k)$ [35,36] or considering only those $\mathbf{k}$ on the Fermi surface [35,36,41], we solve Eq. (8) without further approximation by the power method [43] to find the largest positive eigenvalue $\lambda_{\max}$ and T_c is reached when $\lambda_{\max}$ reaches 1. In this way, the sublattice, momentum, and frequency-dependence of $\phi(k)$ can all be solved self-consistently. The reason why previous studies adopted the above approximations is because solving Eq. (8) straightforwardly is much more time and memory consuming. However, by adopting those approximations, either the frequency dependence of the pairing function or the contribution of those $\mathbf{k}$ points away from the Fermi surface will be lost.

In the iterative process, due to the anticommutation relation of the fermions, the initial input $\phi(k)$ should satisfy

$$\phi^{\alpha\beta}(\mathbf{k}, ip_n) = \phi^{\beta\alpha}(-\mathbf{k}, -ip_n) \tag{11}$$

for spin singlet pairing and

$$\phi^{\alpha\beta}(\mathbf{k}, ip_n) = -\phi^{\beta\alpha}(-\mathbf{k}, -ip_n) \tag{12}$$

for spin triplet pairing.

After convergence, the anomalous self-energy in the band basis $\Delta(k)$ is calculated as

$$\Delta(k) = Q^{\dagger}_{\mathbf{k}} \phi(k) Q^{*}_{-\mathbf{k}} = Q^{\dagger}_{\mathbf{k}} \phi(k) Q_{\mathbf{k}}. \tag{13}$$

Similarly, we should have

$$\Delta^{\alpha\beta}(\mathbf{k}, ip_n) = \Delta^{\beta\alpha}(-\mathbf{k}, -ip_n) \tag{14}$$

for spin singlet pairing and

$$\Delta^{\alpha\beta}(\mathbf{k}, ip_n) = -\Delta^{\beta\alpha}(-\mathbf{k}, -ip_n) \tag{15}$$

for spin triplet pairing.

In the following, we adjust the chemical potential μ in Eq. (1) to ensure the electron filling $\langle n \rangle = (5/12 + 0.02) \times 2$. Here

$$\begin{aligned} \langle n \rangle &= \frac{1}{N_{\text{sublattice}} N} \sum_{\mathbf{k},s,\sigma} \langle c^{\dagger}_{\mathbf{k}s\sigma} c_{\mathbf{k}s\sigma} \rangle \\ &= \frac{2}{N_{\text{sublattice}} N} \sum_{\mathbf{k},s} G^{ss}(\mathbf{k}, -0^+) \\ &= \frac{2T}{N_{\text{sublattice}} N} \sum_{\mathbf{k},s,p_n} G^{ss}(\mathbf{k}, ip_n) e^{ip_n 0^+}, \end{aligned} \tag{16}$$

where $N_{\text{sublattice}}$ denotes the number of sublattices in the unit cell, which is 3 in the present model. Then by using the relation [44]

$$T \sum_{p_n} G^{ss}(\mathbf{k}, ip_n) e^{ip_n 0^+} = \frac{1}{2} + T \sum_{p_n} G^{ss}(\mathbf{k}, ip_n) \tag{17}$$

we have

$$\langle n\rangle = \frac{1}{N_{\text{sublattice}}N}\sum_{\mathbf{k},s} 1 + \frac{2T}{N_{\text{sublattice}}N}\sum_{\mathbf{k},s,p_n} G^{ss}(\mathbf{k}, ip_n)$$
$$= 1 + \frac{2T}{N_{\text{sublattice}}N}\sum_{k,s} G^{ss}(k). \tag{18}$$

The reason we adopt such an electron filling is because, at $\langle n\rangle = 5/12 \times 2$, the Fermi level is located exactly at the upper van Hove singularity at M, and the Fermi surface forms a perfect hexagon. In this case, the Fermi surface is perfectly nested and may lead to various density-wave orders instead of superconductivity. Since we are more concerned with superconductivity, we slightly change the value of $\langle n\rangle$ away from $5/12 \times 2$, so the Fermi level is not located at the van Hove singularity and the Fermi surface is not perfectly nested. In addition, it is experimentally observed that, when the optimal superconductivity is reached, the Fermi level is not at the van Hove singularity [14–16,18,20].

The number of unit cells is set to be $N = 64 \times 64$ and we use 16 384 Matsubara frequencies ($-16\,383\pi T \leqslant p_n \leqslant 16\,383\pi T$ and $-16\,382\pi T \leqslant \omega_n \leqslant 16\,384\pi T$). The temperature T is set to be $T = 0.01$. The summations over momentum and frequency are both done by fast Fourier transformation (FFT).

III. RESULTS AND DISCUSSION

First, in Figs. 1(a) and 1(b) we show the Fermi surface and band structure in our subsequent calculation. At this electron filling, the Fermi surface is not perfectly hexagonal, therefore the nesting condition is less satisfied. It may suppress various density-wave orders related to Fermi surface nesting, while superconductivity can emerge upon their suppression. The chemical potential $\mu \approx 0.08$ is solved according to Eq. (18) and the eigenvalues of Eq. (1) along the high-symmetry directions are shown in Fig. 1(b). The Fermi level (the $E^s_{\mathbf{k}} = 0$ line) is close to the upper van Hove singularity at M.

Second, since the summation of frequency [either p_n in Eq. (6) or ω_n in Eq. (8)] is done by FFT in our calculation, we have to verify that this approximation does not lead to appreciable deviation from the analytical results. This is done by comparing the results obtained by FFT of Eq. (6) and the analytical results of Eq. (7). At a given $q = (\mathbf{q}, i\omega_n)$, χ_0 is a 9×9 Hermitian matrix. We denote its largest eigenvalue as α. In Fig. 1(c), we show α calculated at $\omega_n = 0$, with $\mathbf{q}$ along the high-symmetry directions. We can see that the FFT result of Eq. (6) and the analytical result of Eq. (7) agree with each other, suggesting that the FFT can give reliable χ_0 at $\omega_n = 0$. The largest peak of α is located close to M, and we denote this momentum as $\mathbf{q} = \mathbf{Q}$. Furthermore, in Fig. 1(d) we show α calculated at $\mathbf{q} = \mathbf{Q}$, for varying ω_n. We can see that the FFT and analytical results also agree with each other, with only minor quantitative deviation in the large $|\omega_n|$ region (as denoted by the two rectangles). However in this region, α is extremely small and such a deviation will not affect the following results qualitatively. Besides this region, the two results agree quite well, as shown in the inset of Fig. 1(d). Therefore, we conclude that the FFT used in our calculation can indeed approximate the summation over infinite number of frequencies and that the results presented below are reliable.

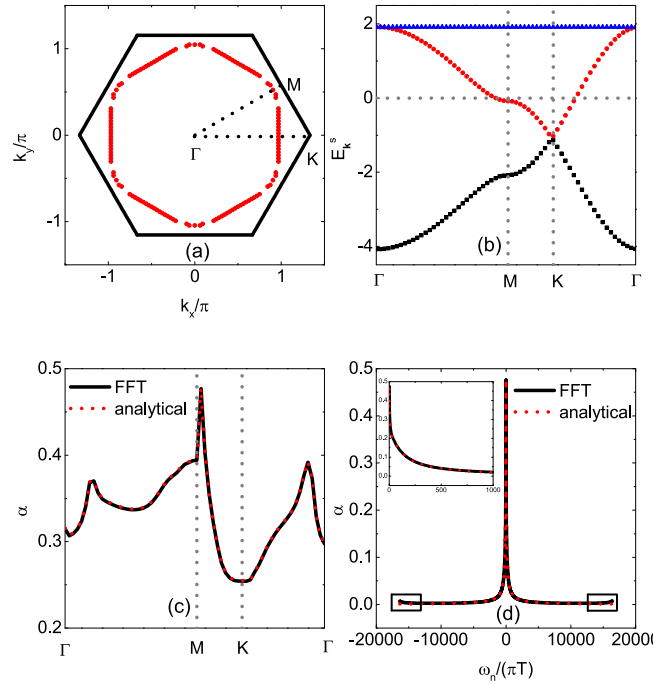

FIG. 1. (a) The Fermi surface at the electron filling $\langle n\rangle = (5/12 + 0.02) \times 2$ (red); the thick black lines are the boundaries of the first Brillouin zone. The black dotted lines indicate the high-symmetry directions. (b) The eigenvalues of Eq. (1) along the high-symmetry directions. (c) The largest eigenvalue of the matrix $\chi_0(\mathbf{q}, i\omega_n = 0)$ along the high-symmetry directions. (d) The largest eigenvalue of $\chi_0(\mathbf{Q}, i\omega_n)$ for varying ω_n. The two rectangles enclose areas where the FFT and analytical results show minor deviation. The inset in (d) shows the largest eigenvalue of $\chi_0(\mathbf{Q}, i\omega_n)$ for $0 \leqslant \omega_n/(\pi T) \leqslant 10^3$.

Then we set the interaction strength U and V as tuning parameters to study their effect on the spin and charge susceptibilities, as well as on the superconducting pairing symmetry. In the following, we set $U = 1, 1.5, 2$, $V = 0.25, 0.5, 1$ and consider their different combinations. For a given $q = (\mathbf{q}, i\omega_n)$, χ_s and χ_c defined in Eq. (A2) are both 9×9 Hermitian matrices and we denote their largest eigenvalues as α_{spin} and α_{charge}, respectively. From Eqs. (A2)–(A4) we can see that α_{spin} depends only on U, but not on V, while α_{charge} depends on both U and V. Figure 2(a) shows α_{spin} calculated at $\omega_n = 0$, with $\mathbf{q}$ along the high-symmetry directions. As U increases, α_{spin} is enhanced, as expected, since it is well known that the on-site Hubbard interaction can enhance the spin susceptibility. In addition, there are three major peaks: one is close to M and the other two are close to Γ. They are all present in the bare susceptibility ($U = 0$) and all get enhanced by increasing U. None of these peaks overwhelmingly wins over the other two, indicating that the momentum structure of the spin susceptibility is highly competing. Figures 2(b) and 2(c) show α_{charge} calculated in the same way as α_{spin} in Fig. 2(a). Generally, the momentum structure of α_{charge} is similar to α_{spin}. However, α_{charge} is suppressed by increasing U and enhanced by increasing V, which is also as expected.

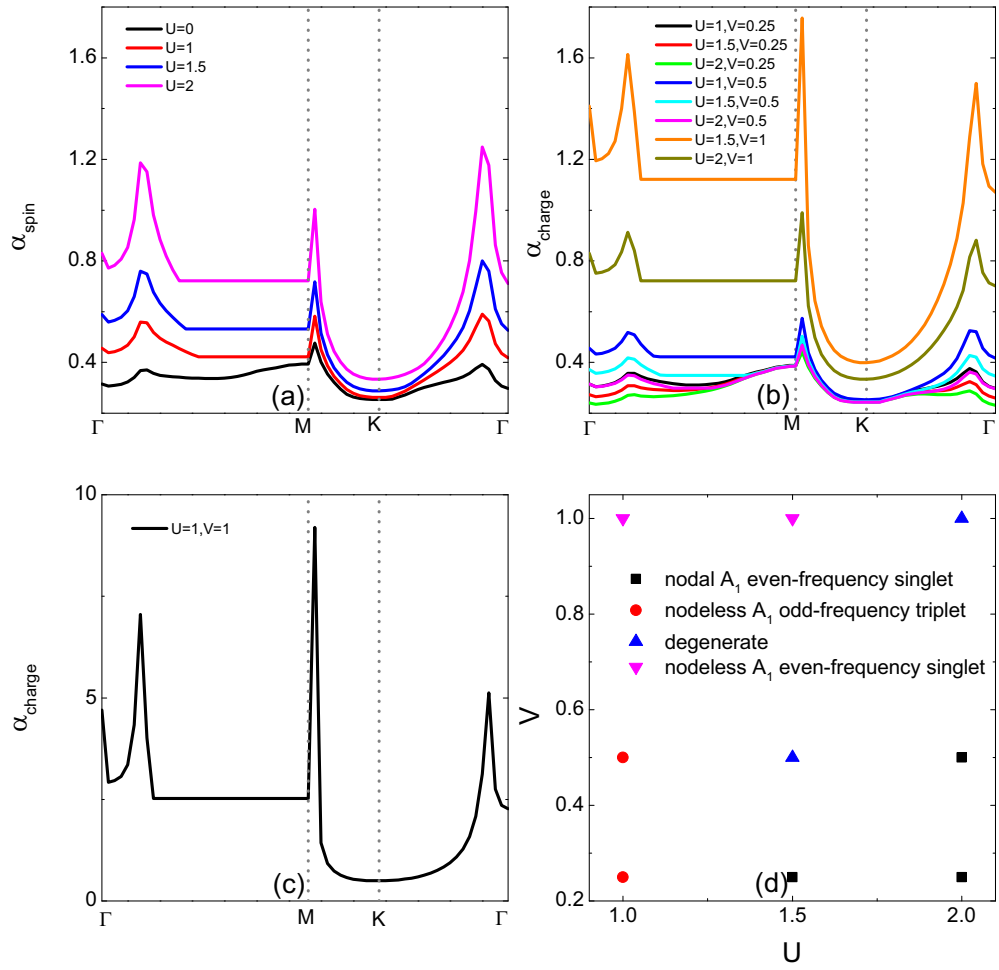

FIG. 2. (a) The largest eigenvalue of the matrix χ_s defined in Eq. (A2), calculated at $\omega_n = 0$ and $\mathbf{q}$ along the high-symmetry directions. (b) and (c) are similar to (a), but for χ_c. (d) The superconducting pairing symmetry as a function of U and V.

For most of the interaction strength, $\alpha_{\text{spin}} > \alpha_{\text{charge}}$, indicating a dominant spin fluctuation over the charge one. However at $(U, V) = (1, 1)$ and (1.5,1), α_{charge} surpasses α_{spin} and in these two cases there appears an appreciable peak located exactly at Γ in α_{charge}.

Finally we come to the superconducting pairing symmetry. As mentioned above, we solve Eq. (8) by using two different pairing interactions, presented in Eqs. (9) and (10), together with two different initial input $\phi(k)$ satisfying Eqs. (11) and (12). Therefore for a given (U, V), we can get two λ_{max}: one for the spin singlet pairing and the other one for the spin triplet pairing. The one with larger λ_{max} is the preferred pairing. Figure 2(d) shows the preferred pairing symmetry as a function of U and V, while the corresponding λ_{max} is shown in Figs. 3(a) and 3(b). Having determined the spin singlet/triplet nature of the pairing, the converged $\phi(k)$ then indicates the pairing function in momentum, frequency and sublattice space. By carefully checking the numerical results, we find that $\phi(k)$ satisfies the following relations:

$$\phi(\mathbf{k}, ip_n) = \begin{cases} \phi(\mathbf{k}, -ip_n) & \text{for spin singlet pairing,} \\ -\phi(\mathbf{k}, -ip_n) & \text{for spin triplet pairing.} \end{cases} \quad (19)$$

That is, the pairing is either spin singlet and even frequency or spin triplet and odd frequency [45]. We then transform $\phi(k)$ to the band basis according to Eq. (13). Since in the present model only band 2 crosses the Fermi level, in the following we show only $\Delta^{22}(\mathbf{k}, ip_n)$ at the lowest positive Matsubara frequency ($p_n = \pi T$), which can approximate the pairing function at the Fermi level.

When the spin fluctuation is much larger than the charge one ($\alpha_{\text{spin}} \gg \alpha_{\text{charge}}$), e.g., at $(U, V) = (2, 0.25)$, spin singlet and even-frequency pairing are preferred. We show

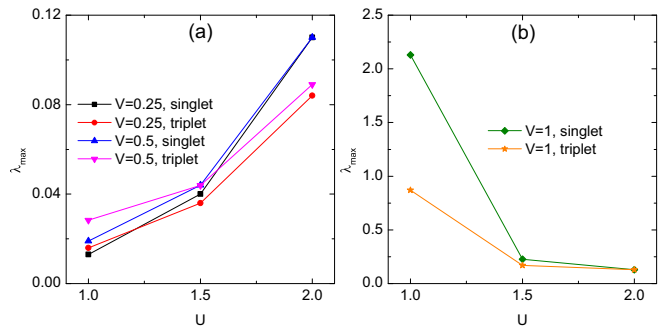

FIG. 3. The largest positive eigenvalue λ_{max} of Eq. (8). (a) is for $U = 1, 1.5, 2$ and $V = 0.25, 0.5$. (b) is for $U = 1, 1.5, 2$ and $V = 1$.

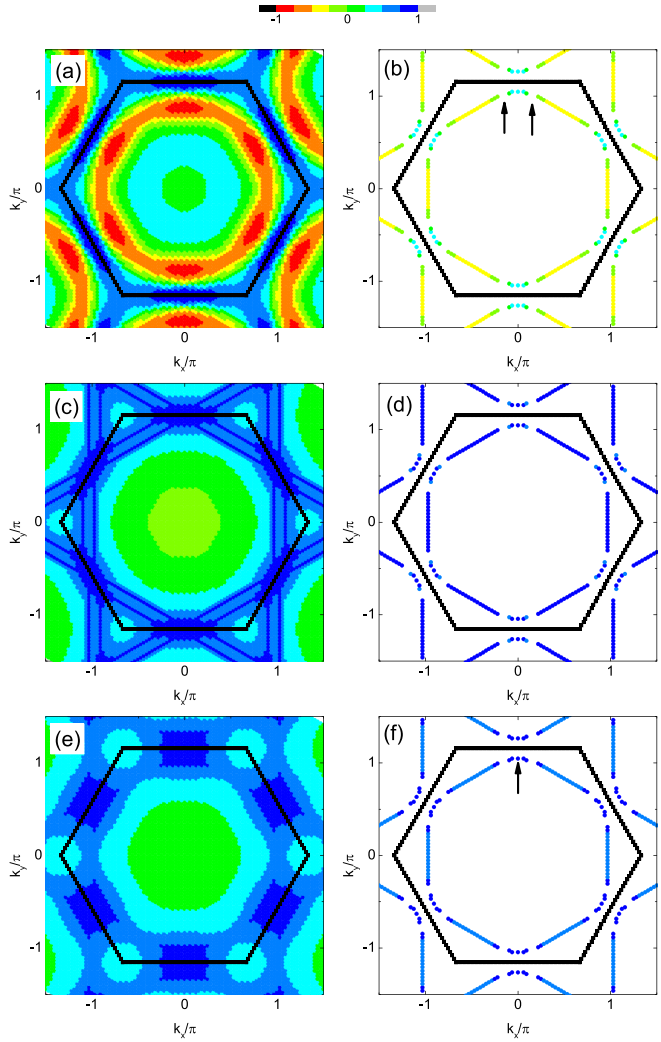

FIG. 4. Left panels: $\Delta^{22}(\mathbf{k}, i\pi T)$ calculated at $(U, V) = (2, 0.25)$ (a), (1,1) (c), and (1,0.5) (e). Right panels: $\Delta^{22}(\mathbf{k}_F, i\pi T)$ calculated at $(U, V) = (2, 0.25)$ (b), (1,1) (d), and (1,0.5) (f). The thick black lines are the boundaries of the first Brillouin zone. The black arrows in (b) denote the gap nodes on the Fermi surface, while the one in (f) indicates the specific Fermi momentum at which we performed a Padé approximation.

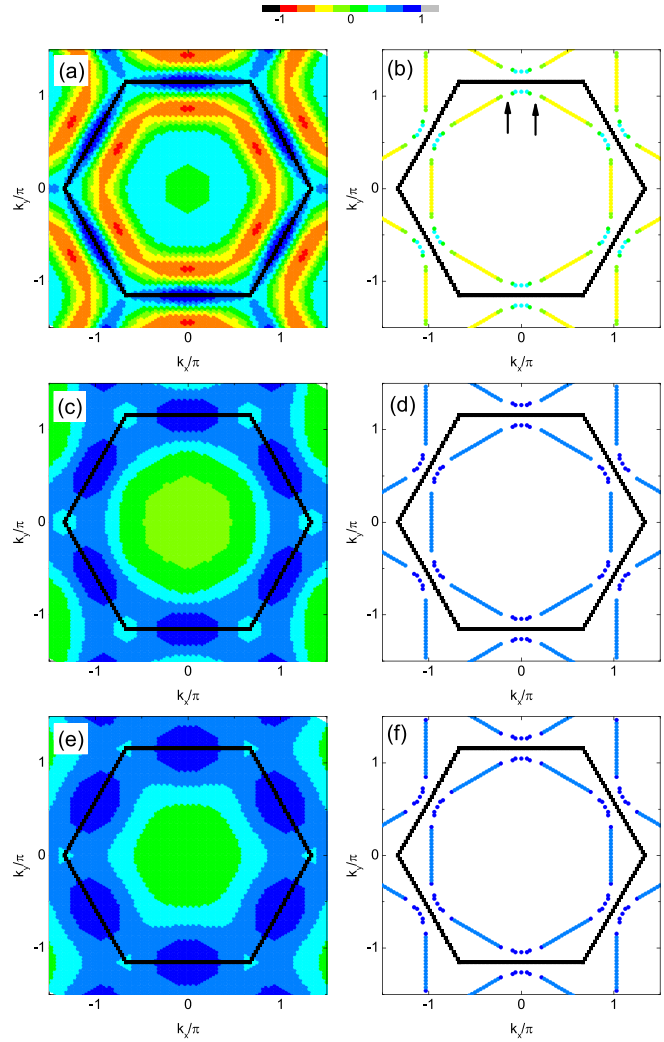

FIG. 5. (a) and (b) are the fitting results of Eqs. (B1), (B2), and (B3). (c) and (d) are the fitting results of Eq. (B4). (e) and (f) are the fitting results of Eq. (B5).

$\Delta^{22}(\mathbf{k}, i\pi T)$ in Fig. 4(a). By using the convention of Ref. [36], we characterize the pairing symmetry in terms of the irreducible representation of the C_{6v} point group, and we can see that the pairing symmetry is A_1 with sign change in the Brillouin zone. On the Fermi surface, there is also sign change in $\Delta^{22}(\mathbf{k}_F, i\pi T)$, where $\mathbf{k}_F$ is the Fermi momentum [see Fig. 4(b)]. There are 12 gap nodes on the Fermi surface, whose locations are denoted by the black arrows and their counterparts by a $\frac{\pi}{3}$ rotation. We denote this pairing as nodal A_1 even-frequency singlet. In this case, $\phi(\mathbf{k}, i\pi T)$ can be fitted to Eqs. (B1)–(B3). The fitting results are shown in Figs. 5(a) and 5(b) for comparison. The pairing is on the same sublattice and is composed of on-site and higher order lattice harmonics between several unit cells.

When the charge fluctuation is much larger than the spin one ($\alpha_{\text{charge}} \gg \alpha_{\text{spin}}$), e.g., at $(U, V) = (1, 1)$, spin singlet and even-frequency pairing are still preferred. $\Delta^{22}(\mathbf{k}, i\pi T)$ shown in Fig. 4(c) suggests the pairing is still A_1, with slight sign change in the Brillouin zone. However on the Fermi surface, there is no sign change in $\Delta^{22}(\mathbf{k}_F, i\pi T)$ [see Fig. 4(d)]. We denote this pairing as nodeless A_1 even-frequency singlet. $\phi(\mathbf{k}, i\pi T)$ can be fitted to Eq. (B4) and the fitting results are shown in Figs. 5(c) and 5(d). It indicates the pairing is also on the same sublattice and is still composed of on-site and higher order lattice harmonics. However in this case, the on-site component is enhanced compared to Eq. (B3).

The above two scenarios can be understood as follows. For spin singlet pairing, the pairing interaction from the spin fluctuation is $\frac{3}{2}U_s\chi_s(q)U_s$. It is repulsive and can lead to a sign-changing gap function on the Fermi surface. Therefore if the spin fluctuation is dominant, we have nodal A_1 even-frequency singlet pairing. On the contrary, the pairing interaction from the charge fluctuation is $-\frac{1}{2}C(\mathbf{q})\chi_c(q)C(\mathbf{q})$. It is attractive and can lead to a sign-preserving gap function on the Fermi surface. Therefore, if the charge fluctuation is dominant, we have nodeless A_1 even-frequency singlet pairing.

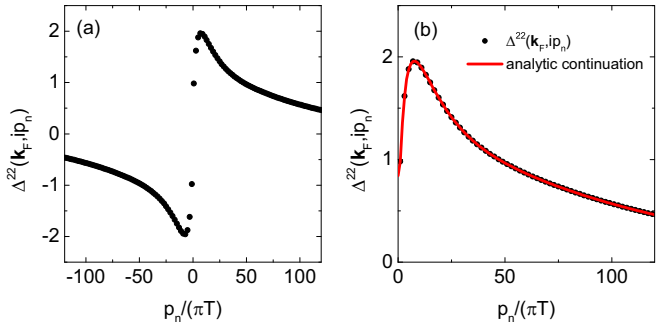

FIG. 6. (a) The frequency dependence of $\Delta^{22}(\mathbf{k}_F, ip_n)$ at a specific $\mathbf{k}_F$ indicated by the black arrow in Fig. 4(f). (b) Analytic continuation of $\Delta^{22}(\mathbf{k}_F, ip_n)$ by means of a 1024-point Padé approximation. The pairing function is the nodeless A_1 odd-frequency triplet at $(U, V) = (1, 0.5)$.

When the spin and charge fluctuations are comparable ($\alpha_{\text{spin}} \approx \alpha_{\text{charge}}$), $\lambda_{\max}$ of the spin triplet pairing can be close to or even larger than that of the spin singlet one. For example, at $(U, V) = (1, 0.5)$, spin triplet and odd-frequency pairing are preferred. In this case, the pairing symmetry is still A_1 and there is no sign change of the pairing function on the Fermi surface [see Figs. 4(e) and 4(f)]. We thus denote this pairing as nodeless A_1 odd-frequency triplet. $\phi(\mathbf{k}, i\pi T)$ in this case can be fitted to Eq. (B5), with the fitting results shown in Figs. 5(e) and 5(f). From Eqs. (B4) and (B5) it can be seen that the nodeless A_1 even-frequency singlet and the nodeless A_1 odd-frequency triplet have similar momentum dependence. However, their frequency dependences are opposite: one is even frequency while the other one is odd frequency. In addition, for this nodeless A_1 odd-frequency triplet, we have verified numerically that the magnitude of $\phi(\mathbf{k}, i\pi T)$ is comparable to the magnitude of $\phi(\mathbf{k}, ip_n)$ with $p_n \neq \pi T$, indicating that the pairing function is finite on the Fermi level and the quasiparticle spectrum is indeed fully gapped. For example, at a specific $\mathbf{k}_F$ indicated by the black arrow in Fig. 4(f), we plot the frequency dependence of $\Delta^{22}(\mathbf{k}_F, ip_n)$ in Fig. 6(a), an odd-frequency dependence is clearly seen. We then use a 1024-point Padé approximation to perform an analytic continuation of $\Delta^{22}(\mathbf{k}_F, ip_n)$ down to $p_n = 0^+$, as shown in Fig. 6(b). Clearly, $\Delta^{22}(\mathbf{k}_F, i0^+) \neq 0$, indicating that $\Delta^{22}(\mathbf{k}_F, ip_n)$ is discontinuous at $p_n = 0$.

This spin-triplet, odd-frequency and even-parity pairing function has not been found in previous studies of the kagome lattice with a similar method [35,36]. Instead they found spin-triplet and odd-parity pairing states such as f-wave and p-wave states. The reason is that, in Refs. [35] and [36], the frequency-dependence of the pairing function is neglected, which means that it is assumed to be even frequency. However, this peculiar pairing state is an allowed one [45] and can show up once the frequency dependence of Eq. (8) is taken into account.

For one single sublattice, e.g., the A sublattice, the pairing function $f_{AA,\mathbf{k}}$ in Eqs. (B3)–(B5) does not respect the A_1 symmetry. However, since

$$\begin{aligned}\Delta^{22}(\mathbf{k}, i\pi T) &= \Delta^{22}(k_1, k_2, i\pi T)\\ &= \sum_{\alpha,\beta} Q^{\dagger 2\alpha}_{\mathbf{k}} \phi^{\alpha\beta}(\mathbf{k}, i\pi T) Q^{\beta 2}_{\mathbf{k}}\\ &= \sum_{\alpha} \left|Q^{\alpha 2}_{\mathbf{k}}\right|^2 \phi^{\alpha\alpha}(\mathbf{k}, i\pi T)\\ &= \left|Q^{12}_{\mathbf{k}}\right|^2 f_{AA}(k_1, k_2) + \left|Q^{22}_{\mathbf{k}}\right|^2 f_{BB}(k_1, k_2)\\ &\quad + \left|Q^{32}_{\mathbf{k}}\right|^2 f_{CC}(k_1, k_2), \end{aligned} \tag{20}$$

the properties $f_{BB,\mathbf{k}} = f_{AA}(k_2, k_1)$ and $f_{CC,\mathbf{k}} = f_{AA}(k_1, k_1 - k_2)$ guarantee that $\Delta^{22}(\mathbf{k}, i\pi T)$ stays invariant as $\mathbf{k}$ rotates $\frac{2\pi}{3}$, leading to the A_1 pairing symmetry in the band basis.

At some values of U and V, e.g., at $(U, V) = (2, 1)$ and (1.5,0.5), nodal A_1 even-frequency singlet and nodeless A_1 odd-frequency triplet are degenerate within our numerical accuracy. Thus we denote these two cases as degenerate in Fig. 2(d).

All the pairing functions $\phi(k)$ we obtained above are real, up to a global phase, thus the superconducting state itself does not break the time-reversal symmetry. In addition, by using the numerical technique called deflation, together with the power method, we can calculate the second largest positive eigenvalue λ_{second} of Eq. (8) and the corresponding $\phi(k)$. For example, at $(U, V) = (2, 0.25)$ and for the spin singlet case, the second largest positive eigenvalue $\lambda_{\text{second}} \approx 0.08$ and the corresponding pairing function $\Delta^{22}(\mathbf{k}, i\pi T)$ are shown in Fig. 7. We can see that the momentum structure of the real and imaginary parts of $\Delta^{22}(\mathbf{k}, i\pi T)$ are different, thus it cannot be taken as real and this pairing function breaks the time-reversal symmetry. However since λ of this pairing is smaller, it is not the preferred pairing compared to the nodal A_1 even-frequency singlet shown in Fig. 4(a).

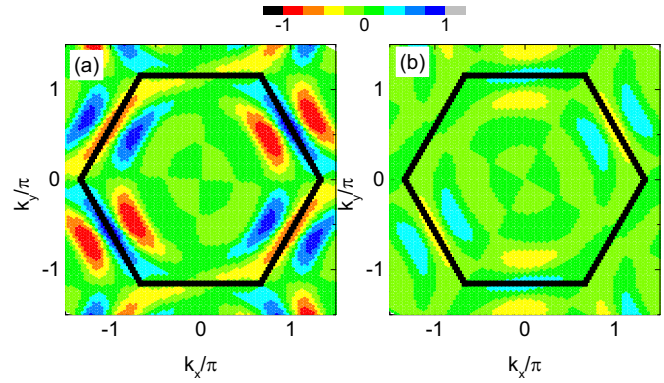

FIG. 7. (a) $\text{Re}\Delta^{22}(\mathbf{k}, i\pi T)$ and (b) $\text{Im}\Delta^{22}(\mathbf{k}, i\pi T)$ corresponding to the second largest positive eigenvalue of Eq. (8), calculated at $(U, V) = (2, 0.25)$ and for the spin singlet case.

IV. SUMMARY

We investigate the possible superconducting pairing in a single-orbital model of the kagome lattice. By taking into account the on-site and nearest-neighbor interactions, the spin and charge fluctuations are obtained based on the RPA. We then solve the full momentum-, sublattice-, and frequency-dependent superconducting pairing function from the linearized Eliashberg equation. Our results suggest that, depending on the values of the interaction strength, there exist two kinds of superconducting pairing: one is spin singlet and even frequency, while the other one is spin triplet and

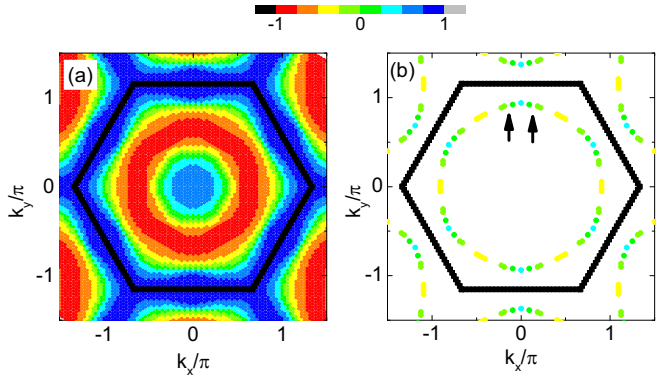

FIG. 8. Similar to Figs. 4(a) and 4(b), but at $\langle n\rangle = (5/12 + 0.06) \times 2$. The black arrows in (b) denote the gap nodes on the Fermi surface.

odd frequency. Although the spin and frequency dependences of these two pairings are opposite, the momentum dependence of both respects A_1 symmetry. This A_1 symmetry is very robust and prevails for moderate interaction strength. In addition, it may be nodal or nodeless, depending on the relative strength of the spin and charge fluctuations. A slight variation of the Fermi surface by doping does not change the main conclusions as well. For example, if the electron filling is increased to $\langle n\rangle = (5/12 + 0.06) \times 2$ (corresponding to further electron-doped case), or decreased to $\langle n\rangle = (5/12 - 0.02) \times 2$ (corresponding to hole-doped case), the size and shape of the Fermi surface will vary slightly. In this case, at $(U, V) = (2, 0.25)$ and for spin singlet pairing, we plot $\Delta^{22}(\mathbf{k}, i\pi T)$ and $\Delta^{22}(\mathbf{k}_F, i\pi T)$ in Figs. 8 and 9. Compared to Figs. 4(a) and 4(b) we can see that the pairing is still nodal A_1 even-frequency singlet. Thus, the A_1 pairing symmetry is not only robust to the interaction strength, but also to slight variation of the Fermi surface.

In the present study, we adopt the RPA, which neglects the renormalization of the normal and anomalous self-energies to the Green's function. In the future, we will use the fluctuation-exchange technique to investigate this effect. Furthermore, the experimental consequences of the possible spin triplet and odd-frequency pairing will also be studied. The odd-frequency order may lead to different Josephson effect as compared to the even-frequency one; see Sec. IV H 1 and references therein in Ref. [45]. For example, the Josephson effect between an odd-frequency superconductor and an even-frequency one may have a different current-phase relation, compared to that of two even-frequency superconductors. In addition, the conductance of a diffusive junction consisting of a normal metal in contact with an s-wave triplet odd-frequency superconductor may also show different behaviors as compared to the even-frequency superconductor. In contrast, the odd-frequency order will not lead to an unusual Meissner response and is thus also thermodynamically stable (see Sec. IV E and references therein in Ref. [45]). Therefore, we propose to use the Josephson junction or normal-metal–superconductor junction to probe the possible odd-frequency order in the kagome superconductors. Here we need to point out that if the frequency dependence is neglected in solving the Eliashberg equation, as in Refs. [35] and [36], the odd-frequency pairing will never show up. Finally, this work presents the preliminary results of the superconducting pairing in a single-orbital kagome lattice; the material specific multiorbital model will also be investigated in detail soon. For example, in Ref. [46], a circular Sb-derived pocket centered around the Γ point is revealed, which might be crucial to understand the superconducting properties of this system. The angle-resolved photoemission spectroscopy (ARPES) data also indicate that the hexagonal-shaped Fermi surface sheet is influenced by t' (substantial curvature). We will investigate these effects in detail in the future.

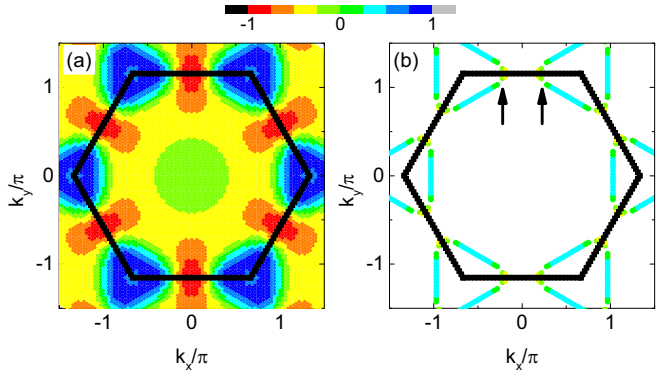

FIG. 9. Similar to Fig. 8, but at $\langle n\rangle = (5/12 - 0.02) \times 2$.

APPENDIX A: RPA METHOD

The irreducible susceptibility is defined as

$$\chi_0^{\alpha\beta,\gamma\delta}(q) = \frac{1}{2N}\int_0^{1/T} d\tau\, e^{i\omega_n\tau} \sum_{\mathbf{k},\mathbf{k}',\sigma,\sigma'} \times \langle T_\tau c^\dagger_{\mathbf{k}+\mathbf{q}\alpha\sigma}(\tau) c_{\mathbf{k}\beta\sigma}(\tau) c^\dagger_{\mathbf{k}'-\mathbf{q}\gamma\sigma'}(0) c_{\mathbf{k}'\delta\sigma'}(0)\rangle. \tag{A1}$$

Within the RPA, the spin and charge susceptibilities are written as [35]

$$\chi_s(q) = [I - \chi_0(q)U_s]^{-1}\chi_0(q),$$
$$\chi_c(q) = [I + \chi_0(q)C(\mathbf{q})]^{-1}\chi_0(q), \tag{A2}$$

where the nonzero matrix elements of U_s and $C(\mathbf{q})$ are

$$U_s^{\alpha\beta,\gamma\delta} = U, \quad \alpha = \gamma = \delta = \beta, \tag{A3}$$

and

$$C^{\alpha\beta,\gamma\delta}(\mathbf{q}) = \begin{cases} U, & \alpha = \gamma = \delta = \beta, \\ 2V[1 + e^{i(q_1 - q_2)}], & \alpha = \beta = 1, \gamma = \delta = 2, \\ 2V(1 + e^{iq_1}), & \alpha = \beta = 1, \gamma = \delta = 3, \\ 2V[1 + e^{-i(q_1 - q_2)}] & \alpha = \beta = 2, \gamma = \delta = 1, \\ 2V(1 + e^{iq_2}), & \alpha = \beta = 2, \gamma = \delta = 3, \\ 2V(1 + e^{-iq_1}), & \alpha = \beta = 3, \gamma = \delta = 1, \\ 2V(1 + e^{-iq_2}), & \alpha = \beta = 3, \gamma = \delta = 2. \end{cases} \tag{A4}$$

Here $q_1 = \mathbf{q}\cdot\mathbf{a}_1$ and $q_2 = \mathbf{q}\cdot\mathbf{a}_2$.

APPENDIX B: FITTING OF $\phi(\mathbf{k}, i\pi T)$

For the cases shown in Fig. 4, $\phi(\mathbf{k}, i\pi T)$ can be fitted to

$$\phi(\mathbf{k}, i\pi T) = \begin{pmatrix} f_{AA,\mathbf{k}} & 0 & 0 \\ 0 & f_{BB,\mathbf{k}} & 0 \\ 0 & 0 & f_{CC,\mathbf{k}} \end{pmatrix}, \tag{B1}$$

where

$$\begin{aligned} f_{AA,\mathbf{k}} &= f_{AA}(k_1, k_2), \\ f_{BB,\mathbf{k}} &= f_{BB}(k_1, k_2) = f_{AA}(k_2, k_1), \\ f_{CC,\mathbf{k}} &= f_{CC}(k_1, k_2) = f_{AA}(k_1, k_1 - k_2). \end{aligned} \tag{B2}$$

At $(U, V) = (2, 0.25)$,

$$\begin{aligned} f_{AA,\mathbf{k}} \approx\ & 0.48 - [\cos(3k_1 - k_2) + \cos(3k_1 - 2k_2)] \\ & + 0.79\cos(2k_1 - k_2) + 0.68\cos(4k_1 - 2k_2) \\ & + 0.52[\cos(4k_1 - k_2) + \cos(4k_1 - 3k_2)] \\ & + 0.44[\cos(k_1 - k_2) + \cos k_1] - 0.26\cos k_2 \\ & - 0.25[\cos(5k_1 - k_2) + \cos(5k_1 - 4k_2)] \\ & - 0.24[\cos(2k_1 - 2k_2) + \cos(2k_1)] \\ & - 0.2[\cos(5k_1 - 2k_2) + \cos(5k_1 - 3k_2)]. \end{aligned} \tag{B3}$$

At $(U, V) = (1, 1)$,

$$\begin{aligned} f_{AA,\mathbf{k}} \approx\ & 1 - 0.84[\cos k_1 + \cos(k_1 - k_2)] \\ & + 0.3[\cos(2k_1) + \cos(2k_1 - 2k_2)] - 0.23\cos k_2 \\ & - 0.16[\cos(3k_1) + \cos(3k_1 - 3k_2)]. \end{aligned} \tag{B4}$$

At $(U, V) = (1, 0.5)$,

$$\begin{aligned} f_{AA,\mathbf{k}} \approx\ & 1 - 0.69[\cos k_1 + \cos(k_1 - k_2)] \\ & + 0.34\cos k_2 + 0.16[\cos(2k_1) + \cos(2k_1 - 2k_2)]. \end{aligned} \tag{B5}$$

[1] B. R. Ortiz, P. M. Sarte, E. M. Kenney, M. J. Graf, S. M. L. Teicher, R. Seshadri, and S. D. Wilson, Superconductivity in the $\mathbb{Z}_2$ kagome metal KV_3Sb_5, Phys. Rev. Mater. **5**, 034801 (2021).

[2] Q. Yin, Z. Tu, C. Gong, Y. Fu, S. Yan, and H. Lei, Superconductivity and normal-state properties of kagome metal RbV_3Sb_5 single crystals, Chin. Phys. Lett. **38**, 037403 (2021).

[3] B. R. Ortiz, S. M. L. Teicher, Y. Hu, J. L. Zuo, P. M. Sarte, E. C. Schueller, A. M. Milinda Abeykoon, M. J. Krogstad, S. Rosenkranz, R. Osborn, R. Seshadri, L. Balents, J. He, and S. D. Wilson, CsV_3Sb_5: A $\mathbb{Z}_2$ topological kagome metal with a superconducting ground state, Phys. Rev. Lett. **125**, 247002 (2020).

[4] H. Zhao, H. Li, B. R. Ortiz, S. M. L. Teicher, T. Park, M. Ye, Z. Wang, L. Balents, S. D. Wilson, and I. Zeljkovic, Cascade of correlated electron states in the kagome superconductor CsV_3Sb_5, Nature (London) **599**, 216 (2021).

[5] K. Y. Chen, N. N. Wang, Q. W. Yin, Z. J. Tu, C. S. Gong, J. P. Sun, H. C. Lei, Y. Uwatoko, and J.-G. Cheng, Double superconducting dome and triple enhancement of T_c in the kagome superconductor CsV_3Sb_5 under high pressure, Phys. Rev. Lett. **126**, 247001 (2021).

[6] Z. Zhang, Z. Chen, Y. Zhou, Y. Yuan, S. Wang, L. Zhang, X. Zhu, Y. Zhou, X. Chen, J. Zhou, and Z. Yang, Pressure-induced reemergence of superconductivity in topological kagome metal CsV_3Sb_5, Phys. Rev. B **103**, 224513 (2021).

[7] X. Chen, X. Zhan, X. Wang, J. Deng, X.-B. Liu, X. Chen, J.-G. Guo, and X. Chen, Highly-robust reentrant superconductivity in CsV_3Sb_5 under pressure, Chin. Phys. Lett. **38**, 057402 (2021).

[8] Y.-X. Jiang, J.-X. Yin, M. M. Denner, N. Shumiya, B. R. Ortiz, G. Xu, Z. Guguchia, J. He, M. S. Hossain, X. Liu, J. Ruff, L. Kautzsch, S. S. Zhang, G. Chang, I. Belopolski, Q. Zhang, T. A. Cochran, D. Multer, M. Litskevich, Z.-J. Cheng *et al.*, Unconventional chiral charge order in kagome superconductor KV_3Sb_5, Nat. Mater. **20**, 1353 (2021).

[9] Z. Liang, X. Hou, F. Zhang, W. Ma, P. Wu, Z. Zhang, F. Yu, J.-J. Ying, K. Jiang, L. Shan, Z. Wang, and X.-H. Chen, Three-dimensional charge density wave and surface-dependent vortex-core states in a kagome superconductor CsV_3Sb_5, Phys. Rev. X **11**, 031026 (2021).

[10] Z. X. Wang, Q. Wu, Q. W. Yin, C. S. Gong, Z. J. Tu, T. Lin, Q. M. Liu, L. Y. Shi, S. J. Zhang, D. Wu, H. C. Lei, T. Dong, and N. L. Wang, Unconventional charge density wave and photoinduced lattice symmetry change in the kagome metal CsV_3Sb_5 probed by time-resolved spectroscopy, Phys. Rev. B **104**, 165110 (2021).

[11] H. Li, G. Fabbris, A. Said, J. Sun, Y.-X. Jiang, J.-X. Yin, Y. Y. Pai, S. Yoon, A. R. Lupini, C. Nelson, Q. W. Yin, C. S. Gong, Z. J. Tu, H. C. Lei, J.-G. Cheng, M. Z. Hasan, Z. Wang, B. Yan, R. Thomale, H. N. Lee *et al.*, Discovery of conjoined charge density waves in the kagome superconductor CsV_3Sb_5, Nat. Commun. **13**, 6348 (2022).

[12] Q. Xiao, Y. Lin, Q. Li, X. Zheng, S. Francoual, C. Plueckthun, W. Xia, Q. Qiu, S. Zhang, Y. Guo, J. Feng, and Y. Peng, Coexistence of multiple stacking charge density waves in kagome superconductor CsV_3Sb_5, Phys. Rev. Res. **5**, L012032 (2023).

[13] J. Frassineti, P. Bonfá, G. Allodi, E. Garcia, R. Cong, B. R. Ortiz, S. D. Wilson, R. D. Renzi, V. F. Mitrović, and S. Sanna, Microscopic nature of the charge-density wave in the kagome superconductor RbV_3Sb_5, Phys. Rev. Res. **5**, L012017 (2023).

[14] Y. Liu, Y. Wang, Y. Cai, Z. Hao, X.-M. Ma, L. Wang, C. Liu, J. Chen, L. Zhou, J. Wang, S. Wang, H. He, Y. Liu, S. Cui, B. Huang, J. Wang, C. Chen, and J.-W. Mei, Doping evolution of superconductivity, charge order, and band topology in hole-doped topological kagome superconductors $Cs(V_{1-x}Ti_x)_3Sb_5$, Phys. Rev. Mater. **7**, 064801 (2023).

[15] Y. M. Oey, F. Kaboudvand, B. R. Ortiz, R. Seshadri, and S. D. Wilson, Tuning charge density wave order and superconductivity in the kagome metals $KV_3Sb_{5-x}Sn_x$ and $RbV_3Sb_{5-x}Sn_x$, Phys. Rev. Mater. **6**, 074802 (2022).

[16] Y. M. Oey, B. R. Ortiz, F. Kaboudvand, J. Frassineti, E. Garcia, R. Cong, S. Sanna, V. F. Mitrović, R. Seshadri, and S. D. Wilson, Fermi level tuning and double-dome superconductivity in the kagome metal $CsV_3Sb_{5-x}Sn_x$, Phys. Rev. Mater. **6**, L041801 (2022).

[17] Y. Liu, C.-C. Liu, Q.-Q. Zhu, L.-W. Ji, S.-Q. Wu, Y.-L. Sun, J.-K. Bao, W.-H. Jiao, X.-F. Xu, Z. Ren, and G.-H. Cao, Enhancement of superconductivity and suppression of charge-density wave in As-doped CsV_3Sb_5, Phys. Rev. Mater. **6**, 124803 (2022).

[18] T. Kato, Y. Li, K. Nakayama, Z. Wang, S. Souma, F. Matsui, M. Kitamura, K. Horiba, H. Kumigashira, T. Takahashi, Y. Yao, and T. Sato, Fermiology and origin of T_c enhancement in a kagome superconductor $Cs(V_{1-x}Nb_x)_3Sb_5$, Phys. Rev. Lett. **129**, 206402 (2022).

[19] M. Liu, T. Han, X. Hu, Y. Tu, Z. Zhang, M. Long, X. Hou, Q. Mu, and L. Shan, Evolution of superconductivity and charge density wave through Ta and Mo doping in CsV_3Sb_5, Phys. Rev. B **106**, L140501 (2022).

[20] Y. Li, Q. Li, X. Fan, J. Liu, Q. Feng, M. Liu, C. Wang, J.-X. Yin, J. Duan, X. Li, Z. Wang, H.-H. Wen, and Y. Yao, Tuning the competition between superconductivity and charge order in the kagome superconductor $Cs(V_{1-x}Nb_x)_3Sb_5$, Phys. Rev. B **105**, L180507 (2022).

[21] N. N. Wang, K. Y. Chen, Q. W. Yin, Y. N. N. Ma, B. Y. Pan, X. Yang, X. Y. Ji, S. L. Wu, P. F. Shan, S. X. Xu, Z. J. Tu, C. S. Gong, G. T. Liu, G. Li, Y. Uwatoko, X. L. Dong, H. C. Lei, J. P. Sun, and J.-G. Cheng, Competition between charge-density-wave and superconductivity in the kagome metal RbV_3Sb_5, Phys. Rev. Res. **3**, 043018 (2021).

[22] H. Chen, H. Yang, B. Hu, Z. Zhao, J. Yuan, Y. Xing, G. Qian, Z. Huang, G. Li, Y. Ye, S. Ma, S. Ni, H. Zhang, Q. Yin, C. Gong, Z. Tu, H. Lei, H. Tan, S. Zhou, C. Shen *et al.*, Roton pair density wave in a strong-coupling kagome superconductor, Nature (London) **599**, 222 (2021).

[23] C. C. Zhao, L. S. Wang, W. Xia, Q. W. Yin, J. M. Ni, Y. Y. Huang, C. P. Tu, Z. C. Tao, Z. J. Tu, C. S. Gong, H. C. Lei, Y. F. Guo, X. F. Yang, and S. Y. Li, Nodal superconductivity and superconducting domes in the topological Kagome metal CsV_3Sb_5, arXiv:2102.08356.

[24] G. Ding, H. Wo, Y. Gu, Y. Gu, and J. Zhao, Effect of chromium doping on superconductivity and charge density wave order in the kagome metal $Cs(V_{1-x}Cr_x)_3Sb_5$, Phys. Rev. B **106**, 235151 (2022).

[25] W. Duan, Z. Nie, S. Luo, F. Yu, B. R. Ortiz, L. Yin, H. Su, F. Du, A. Wang, Y. Chen, X. Lu, J. Ying, S. D. Wilson, X. Chen, Y. Song, and H. Yuan, Nodeless superconductivity in the kagome metal CsV_3Sb_5, Sci. China Phys. Mech. Astron. **64**, 107462 (2021).

[26] H.-S. Xu, Y.-J. Yan, R. Yin, W. Xia, S. Fang, Z. Chen, Y. Li, W. Yang, Y. Guo, and D.-L. Feng, Multiband superconductivity with sign-preserving order parameter in kagome superconduc tor CsV_3Sb_5, Phys. Rev. Lett. **127**, 187004 (2021).

[27] R. Gupta, D. Das, C. H. Mielke III, Z. Guguchia, T. Shiroka, C. Baines, M. Bartkowiak, H. Luetkens, R. Khasanov, Q. Yin, Z. Tu, C. Gong, and H. Lei, Microscopic evidence for anisotropic multigap superconductivity in the CsV_3Sb_5 kagome superconductor, npj Quantum Mater. **7**, 49 (2022).

[28] M. Roppongi, K. Ishihara, Y. Tanaka, K. Ogawa, K. Okada, S. Liu, K. Mukasa, Y. Mizukami, Y. Uwatoko, R. Grasset, M. Konczykowski, B. R. Ortiz, S. D. Wilson, K. Hashimoto, and T. Shibauchi, Bulk evidence of anisotropic s-wave pairing with no sign change in the kagome superconductor CsV_3Sb_5, Nat. Commun. **14**, 667 (2023).

[29] C. Mu, Q. Yin, Z. Tu, C. Gong, H. Lei, Z. Li, and J. Luo, S-wave superconductivity in kagome metal CsV_3Sb_5 revealed by $^{121/123}$Sb NQR and ^{51}V NMR Measurements, Chin. Phys. Lett. **38**, 077402 (2021).

[30] Z. Guguchia, C. Mielke III, D. Das, R. Gupta, J.-X. Yin, H. Liu, Q. Yin, M. H. Christensen, Z. Tu, C. Gong, N. Shumiya, M. S. Hossain, T. Gamsakhurdashvili, M. Elender, P. Dai, A. Amato, Y. Shi, H. C. Lei, R. M. Fernandes, M. Z. Hasan, H. Luetkens *et al.*, Tunable unconventional kagome superconductivity in charge ordered RbV_3Sb_5 and KV_3Sb_5, Nat. Commun. **14**, 153 (2023).

[31] Z. Shan, P. K. Biswas, S. K. Ghosh, T. Tula, A. D. Hillier, D. Adroja, S. Cottrell, G.-H. Cao, Y. Liu, X. Xu, Y. Song, H. Yuan, and M. Smidman, Muon spin relaxation study of the layered kagome superconductor CsV_3Sb_5, Phys. Rev. Res. **4**, 033145 (2022).

[32] E. T. Ritz, H. S. Røising, M. H. Christensen, T. Birol, B. M. Andersen, and R. M. Fernandes, Superconductivity from orbital-selective electron-phonon coupling in AV_3Sb_5, Phys. Rev. B **108**, L100510 (2023).

[33] C. Wang, Y. Jia, Z. Zhang, and J.-H. Cho, Phonon-mediated *s*-wave superconductivity in the kagome metal CsV_3Sb_5 under pressure, Phys. Rev. B **108**, L060503 (2023).

[34] C. Wang, S. Liu, H. Jeon, Y. Jia, and J.-H. Cho, Charge density wave and superconductivity in the kagome metal CsV_3Sb_5 around a pressure-induced quantum critical point, Phys. Rev. Mater. **6**, 094801 (2022).

[35] X. Wu, T. Schwemmer, T. Müller, A. Consiglio, G. Sangiovanni, D. D. Sante, Y. Iqbal, W. Hanke, A. P. Schnyder, M. M. Denner, M. H. Fischer, T. Neupert, and R. Thomale, Nature of unconventional pairing in the kagome superconductors AV_3Sb_5 (A = K, Rb, Cs), Phys. Rev. Lett. **127**, 177001 (2021).

[36] A. T. Rømer, S. Bhattacharyya, R. Valentí, M. H. Christensen, and B. M. Andersen, Superconductivity from repulsive interactions on the kagome lattice, Phys. Rev. B **106**, 174514 (2022).

[37] W.-S. Wang, Z.-Z. Li, Y.-Y. Xiang, and Q.-H. Wang, Competing electronic orders on kagome lattices at van Hove filling, Phys. Rev. B **87**, 115135 (2013).

[38] M. L. Kiesel, C. Platt, and R. Thomale, Unconventional fermi surface instabilities in the kagome Hubbard model, Phys. Rev. Lett. **110**, 126405 (2013).

[39] S.-L. Yu and J.-X. Li, Chiral superconducting phase and chiral spin-density-wave phase in a Hubbard model on the kagome lattice, Phys. Rev. B **85**, 144402 (2012).

[40] M. L. Kiesel and R. Thomale, Sublattice interference in the kagome Hubbard model, Phys. Rev. B **86**, 121105(R) (2012).

[41] R. Tazai, Y. Yamakawa, S. Onari, and H. Kontani, Mechanism of exotic density-wave and beyond-Migdal unconventional superconductivity in kagome metal AV_3Sb_5 (A = K, Rb, Cs), Sci. Adv. **8**, eabl4108 (2022).

[42] T. Takimoto, T. Hotta, and K. Ueda, Strong-coupling theory of superconductivity in a degenerate Hubbard model, Phys. Rev. B **69**, 104504 (2004).

[43] S. Andrilli and D. Hecker, *Elementary Linear Algebra*, 5th ed. (Academic, New York, 2016).

[44] See Eqs. (3.5), (3.239), and (3.240), G. D. Mahan, *Many- Particle Physics*, 3rd ed. (Springer, New York, 2000).

[45] J. Linder and A. V. Balatsky, Odd-frequency superconductivity, Rev. Mod. Phys. **91**, 045005 (2019).

[46] M. Kang, S. Fang, J.-K. Kim, B. R. Ortiz, S. H. Ryu, J. Kim, J. Yoo, G. Sangiovanni, D. D. Sante, B.-G. Park, C. Jozwiak, A. Bostwick, E. Rotenberg, E. Kaxiras, S. D. Wilson, J.-H. Park, and R. Comin, Twofold van Hove singularity and origin of charge order in topological kagome superconductor CsV_3Sb_5, Nat. Phys. **18**, 301 (2022).